



Analysis of OECD/NEA medium 1000 MWth sodium-cooled fast reactor using the Monte Carlo serpent code and ENDF/B-VIII.0 nuclear data library

Fatima I. Al-Hamadi¹ · Bassam A. Khuwaileh¹ · Peng Hong Liem^{2,3} · Donny Hartanto¹

Received: 19 May 2020 / Revised: 14 September 2020 / Accepted: 28 October 2020 / Published online: 4 December 2020
© China Science Publishing & Media Ltd. (Science Press), Shanghai Institute of Applied Physics, the Chinese Academy of Sciences, Chinese Nuclear Society and Springer Nature Singapore Pte Ltd. 2020

Abstract This study presents a benchmark evaluation of the new ENDF/B-VIII.0 nuclear data library for the Organization for Economic Co-operation and Development/Nuclear Energy Agency Medium 1000 MWth sodium-cooled fast reactor (SFR). The study presented herein covers both SFR core types, i.e., metallic fueled (MET-1000) and oxide fueled (MOX-1000), simulated using the continuous-energy Monte Carlo Serpent2 code. The neutronics performances of the ENDF/B-VIII.0-based simulations were compared mainly to two libraries: ENDF/B-VII.1 and JENDL-4.0. The comparison includes several neutronics parameters evaluated for the beginning and end of the cycle conditions. These parameters include the effective multiplication factor k_{eff} , total effective delayed neutron fraction β_{eff} , sodium void reactivity ($\Delta\rho_{\text{Na}}$), Doppler constant ($\Delta\rho_{\text{Doppler}}$), and control rod worth ($\Delta\rho_{\text{CR}}$). In addition, a sensitivity study was used to reveal the major isotope/reaction pairs contributing to the discrepancy

observed in the performance of the three libraries using 33 and 44-energy-group structures.

Keywords Serpent · ENDF/B-VIII.0 · Sodium-cooled fast reactor · Sensitivity analysis

1 Introduction

Under the working party of the Organization for Economic Co-operation and Development/Nuclear Energy Agency (OECD/NEA), a neutronics benchmark study of the Generation-IV sodium-cooled fast reactor (SFR) concepts has been conducted and published using different methods and codes [1–3] in conjunction with various nuclear data libraries such as ENDF/B-VII.0 [4], ENDF/B-VII.1 [5], JEFF-3.1 [6], and JENDL-4.0 [7]. The benchmark consists of large 3600 MWth carbide and oxide cores as well as medium 1000 MWth metallic and oxide cores. In this study, the medium SFR cores were calculated using the new version of the nuclear data library, ENDF/B-VIII.0 [8]. The newer library has achieved improvements in many neutron cross section libraries, including the cross sections of materials that are commonly used in the SFR, such as U-235 and Pu-239 in the fuel, Fe-56 in the clad, and O-16 in mixed oxide fuel. Because the accuracy of the nuclear data is extremely important for the design and safety of a nuclear reactor, the impact of the new ENDF/B-VIII.0 on the neutronics and kinetics parameters of an OECD/NEA Medium 1000 MWth SFR was investigated. Both metallic and oxide cores are considered to distinguish the impact of the neutron spectrum.

Several important neutronics parameters are evaluated in the present study, including the effective neutron

This work was supported by the Research Institute of Science and Engineering at the University of Sharjah (No. 1802040790-P).

✉ Donny Hartanto
dhartanto@sharjah.ac.ae

¹ Department of Mechanical and Nuclear Engineering, University of Sharjah, P.O. BOX 27272, Sharjah, United Arab Emirates

² Graduate School of Engineering, Cooperative Major in Nuclear Energy, Tokyo City University (TCU), 1-28-1 Tamazutsumi, Setagaya, Tokyo, Japan

³ Scientific Computational Division, Nippon Advanced Information Service (NAIS Co., Inc.), 416 Muramatsu, Tokaimura, Ibaraki, Japan

multiplication factor k , total effective delayed neutron fraction β_{eff} , prompt neutron generation time Λ , Doppler constant K_D , coolant void reactivity (CVR), and control rod (CR). Each parameter is calculated at the beginning of cycle (BOC) and end of cycle (EOC) using the continuous-energy Monte Carlo Serpent2 code [9]. Three different modern nuclear data libraries are considered: ENDF/B-VIII.0, ENDF/B-VII.1, and JENDL-4.0. In addition to an inter-library comparison, the calculated results are also compared to the results reported by the working group [3]. It should be noted that the reported result is an average value computed by different calculation methods, including deterministic and stochastic methods, and various nuclear data libraries.

2 SFR: core description

The layout of the metallic core is illustrated in Fig. 1. The core consists of inner and outer fuel regions surrounded by reflectors and shielding. The inner core region has 78 fuel subassemblies, and the outer core region has 102 fuel subassemblies. Meanwhile, there were 114 reflector subassemblies, 66 shielding subassemblies, 15 primary control subassemblies, and 4 secondary control subassemblies. The fuel consists of irradiated U-10Zr metallic fuel and is contained in HT-9 cladding. The total core height is 480.20 cm, and the active core height is approximately 85.82 cm. In the calculation, the temperature of the fuel was 534 °C, and the temperature of the coolant and structural material was 432.5 °C.

In Fig. 2, the radial layout of the oxide core is shown. The core has three fuel regions, which are the inner, middle, and outer regions. The fuel is irradiated UO_2 -(TRU)- O_2 contained in the HT-9 clad. There are 30 inner fuel subassemblies, 90 mid-fuel subassemblies, and 60 outer fuel subassemblies. Meanwhile, the number of non-fuel subassemblies is the same as that in the metallic core. The

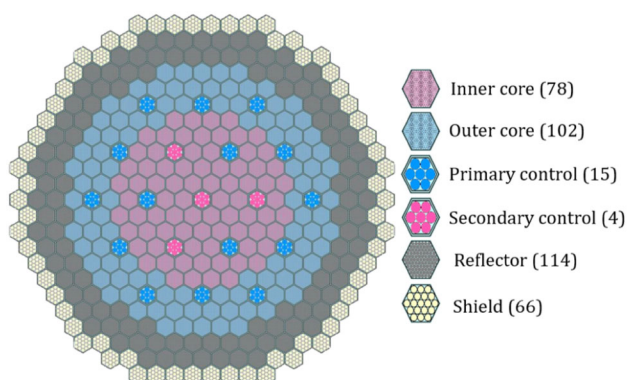


Fig. 1 (Color online) Radial layout of metallic core [1]

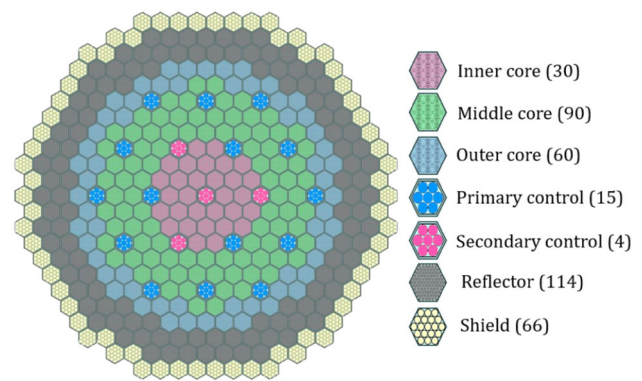


Fig. 2 (Color online) Radial layout of oxide core [1]

total core height is also the same as in the metallic core; however, the active core is slightly taller, at approximately 114.94 cm. The fuel temperature is also higher, at approximately 1027 °C, and the other components have the same temperatures as in the metallic core. For detailed information on the benchmark, including the material compositions and assembly dimensions, readers can refer to [1].

3 ENDF/B-VIII.0 nuclear data library

Under the coordination of the Cross Section Evaluation Working Group (CSEWG), the new ENDF/B-VIII.0 library was released in 2018 [8] and issued in both formats: the traditional ENDF-6 format and the new Generalized Nuclear Database Structure (GNDS) format. This version has represented the most noticeable changes to the ENDF library among all of the previously released versions, which improved the nuclear reaction data library by using the CIELO-project cross sections, new standards, and thermal scattering data, as a result of full co-operation with the new IAEA standards. The updates in the library involve an updated neutron reaction on the structural materials, minor actinides, dosimetry cross sections, decay data, fission energy release, light nuclei, charged-particle reactions, and thermal neutron scattering data. The major highlighted and included changes in the ENDF/B-VIII.0 are summarized in Table 1.

Moreover, a wider energy range was considered as a standard by adding the integral cross section of $^{235}\text{U}(n,f)$ from 7.8–11 eV, the 30 keV Maxwellian-averaged cross section of $\text{Au}(n,\gamma)$, and the higher energy fission reference cross sections from 200 MeV to 1 GeV for $^{235}\text{U}(n,f)$ and $^{238}\text{U}(n,f)$, and from 20 MeV to 1 GeV for $^{209}\text{Bi}(n,f)$ and $^{\text{nat}}\text{Pb}(n,f)$ [8]. The neutron sub-library was expanded to include 557 evaluations, which is 32% of the increment [8]. In return, these changes have a direct impact

Table 1 Major changes in ENDF/B-VIII.0

Category	Changed isotopes
CIELO evaluation	^1H , ^{16}O , ^{56}Fe , ^{235}U , ^{238}U , ^{239}Pu , including prompt fission neutron spectra (PFNS) and prompt fission gamma spectra (PEGS)
Light elements	^2H , ^3He , ^6Li , ^9Be , ^{10}B , $^{12,13}\text{C}$, $^{35,37}\text{Cl}$, and ^{18}O
Structural materials	^{40}Ca , $^{54,56,57,58}\text{Fe}$, $^{58-62,64}\text{Ni}$, ^{59}Co , $^{63,65}\text{Cu}$, $^{174-182}\text{Hf}$, $^{182-186}\text{W}$, ^{105}Rh , and ^{132}Te
Nobel gases	^{40}Ar , ^{78}Kr , ^{124}Xe , and $^{20-22}\text{Ne}$
Minor actinides	$^{236\text{m}}\text{Np}$, ^{240}Pu , and $^{241,243}\text{Am}$
Misc. materials	$^{73-75}\text{As}$, ^{197}Au , and $^{190-198}\text{Pt}$
Unstable isotopes	$T_{1/2} \geq 1$ isotopes
Primary gammas	^6Li , ^{11}B , ^{19}F , ^{23}Na , ^{27}Al , ^{28}Si and $^{35,37}\text{Cl}$

on the simulations of nuclear criticality. In this study, a comparison of using ENDF/B-VIII.0, ENDF/B-VII.1, and JENDL-4.0 in simulating the nuclear performance of the SFR to see the impact of implementing the new library in contrast with the previous libraries.

4 Methodology

4.1 Monte Carlo SERPENT2 code

In this study, a multi-purpose three-dimensional continuous-energy Monte Carlo particle transport code, Serpent2, was used to simulate the neutronics behavior of SFR metallic and oxide cores using the new ENDF/B-VIII.0 library, ENDF/B-VII.1, and JENDL-4.0. The development of Serpent2 was started in 2010 by the VTT Technical Research Centre of Finland [9].

The transport simulation by Serpent2 was conducted based on the k -eigenvalue criticality source method, which limits its applications to a self-sustaining system. The code evaluates the kinetic and delayed neutron parameters automatically, in addition to the entire few group constants required for a coupled nodal diffusion calculation. Based on the user interest, the reaction rate and integral flux detectors for specific regions can be defined and inserted into the code using tallies. Serpent2 is also capable of calculating the sensitivities of various responses to various perturbations using the collision history method and its corresponding uncertainty using the user-provided covariance data. Moreover, the user can construct a 2D or 3D fuel or reactor geometry configuration, where Serpent2 applies the universe-based constructive solid geometry model (CSG) [10]. For particle transportation, a collection of the classical surface tracking is used, in addition to the Woodcock delta-tracking method, which is implemented when the given dimensions are smaller than the mean free

path of the particles [11]. The interaction physics in Serpent2 depends on the ENDF reaction laws, the conventional collision kinematics, the Doppler-broadening rejection correction (DBRC) method, which treats the free-gas scattering kernel close to resonances [12], and probability table sampling for the unsolved resonance region. In addition, the continuous-energy cross sections are provided using ACE format libraries.

4.2 Focus of the current study

In this study, the impact of the changes in the new ENDF/B-VIII.0 on the neutronics and kinetics parameters of an OECD/NEA Medium 1000 MWth SFR as compared to the implementation of older libraries, ENDF/B-VII.1, and JENDL-4.0, was investigated. Several simulations were conducted using the Serpent2 code to evaluate the important neutronics parameters, such as the effective neutron multiplication factor k_{eff} , total effective delayed neutron fraction β_{eff} , prompt neutron generation time Λ , Doppler constant K_D , CVR, and CR. A depletion study was conducted, and the BOC and EOC cores were studied. In addition, a sensitivity study was simulated to see the differences between using a 33-energy group and a 44-energy group for each library considered. The 33-energy group is the typical energy group used in the fast reactor analysis [13], and the 44-energy group is the energy group used in the covariance data.

5 Results and discussion

The Monte Carlo Serpent2 code was used to produce the subsequent results. In the calculation, the sub-assembly in the core was explicitly modeled. Each calculation used 100,000 neutron histories and 1050 total neutron cycles

with 50 inactive cycles. Using this calculation condition, the standard deviation of k_{eff} is approximately 7 pcm.

5.1 Multiplication factor at BOC and EOC

The effective neutron multiplication factor k_{eff} values for the metallic and oxide cores at the BOC and EOC are summarized in Tables 2, 3 respectively. Comparing among the different libraries, JENDL-4.0 provides the highest k_{eff} value of the metallic core at the BOC and EOC than those by ENDF/B-VII.0 and ENDF/B-VII.1. Meanwhile, both JENDL-4.0 and ENDF/B-VII.1 produce a similar k_{eff} , and are higher than those produced by ENDF/VIII.0 for the oxide core. It should be noted that the calculated k_{eff} values are lower than those reported [3].

The value of k_{eff} at the EOC was taken from the depletion results at 328.5 days. In the burnup calculation, the corresponding decay and neutron fission yield libraries of each nuclear data were used. Figures 3, 4 show k_{eff} as a function of burnup. The change of k_{eff} during burnup is linear for each nuclear data because the cross sections of the fission products in the fast spectrum are not as large as in the thermal spectrum. The neutron spectra for each library for the metallic and oxide cores are also illustrated in Figs. 5, 6. It should be noted that the difference in the neutron spectra can reach approximately 20% within the resonance energy region.

5.2 Sensitivity coefficient of multiplication factor

The sensitivity coefficients of k_{eff} for the metallic and oxide cores are shown in Figs. 7, 8, respectively. Serpent2 calculated the sensitivity coefficients based on the collision history-based approach [14]. The sensitivity coefficients are consistent among different nuclear data libraries. It should be noted that Pu-239 (n,f), U-238 (n,f), Pu-240 (n,f), and Pu-241 (n,f) give large positive sensitivities for both cores. Meanwhile, U-238 (n,g) and ($n,inel$) dominate the negative sensitivities for the metallic core. By contrast, the large negative sensitivities for the oxide core include U-238 (n,g) and ($n,inel$), Pu-239 (n,g), O-16 (n,el), Pu-240 (n,g), and Fe-56 ($n,inel$).

5.3 k_{eff} sensitivity

An analysis for evaluating the impact of the ENDF/B-VIII.0 library was also conducted by replacing a single isotope from the old library with a new one from the ENDF/B-VIII.0 library at BOC, which is summarized in Tables 4, 5. It should be noted that there are significant changes in k_{eff} from Fe-56 and U-238 of ENDF/B-VII.1 and Fe-56 and Pu-239 of JENDL-4.0 for both cores. A detailed study was then conducted to evaluate the contribution of each isotope/reaction pair to the change in k_{eff} by comparing the results of the new library ENDF/B-VIII.0 with JENDL-4.0 and ENDF/B-VII.1. If the k_{eff} sensitivity coefficient S_{σ} is defined as follows:

$$S_{\sigma} = \frac{\sigma}{k_{\text{eff}}} \frac{dk_{\text{eff}}}{d\sigma}, \quad (1)$$

where σ is the multigroup microscopic cross section obtained from Serpent2. Then, the first-order estimation of the k_{eff} change can be calculated using Eq. (2), where $\Delta\sigma$ is the difference in the cross section (between different libraries), and S_{σ} is the energy-dependent sensitivity coefficient obtained by Serpent2.

$$\Delta k_{\text{eff}} = \frac{k_{\text{eff}}}{\sigma} \times S_{\sigma} \times \Delta\sigma \quad (2)$$

The results of the major contributors to k_{eff} of Fe-56, U-238, and Pu-239 were obtained for the metallic and oxide SFR core. Moreover, the difference between utilizing a 44-energy group or a 33-energy group of cross sections and S_{σ} on the k_{eff} was also investigated. Table 6 through Table 9 summarize the results of each isotope contribution to k_{eff} in total (in the resultant change column). The individual reaction contributions of each isotope are also shown. The resultant change is defined as the summation of the reaction contribution for each isotope to k_{eff} .

The results of the metallic core summarized in Tables 6, 7 illustrate an increase in k_{eff} when using ENDF/B-VII.1 compared to the new library ENDF/B-VIII.0 (for both group structures). The cross section of U-238 from ENDF/B-VIII.0 increases the k_{eff} by approximately 175 pcm and 135 pcm when analyzed using the 44-energy group and 33-energy group, respectively, and the major reactions are of U-238 (n,f) and (n,g). Similarly, the cross section of Pu-239 from ENDF/B-VIII.0 increases the k_{eff} by

Table 2 k_{eff} of metallic core at the BOC and EOC

Library	k_{eff} at BOC	k_{eff} at EOC
ENDF/B-VIII.0	1.02993 ± 0.00007	1.00580 ± 0.00007
ENDF/B-VII.1	1.02808 ± 0.00007	1.00522 ± 0.00007
JENDL-4.0	1.03240 ± 0.00007	1.00893 ± 0.00007
Reported result (average) [3]	1.03578 ± 0.0078	1.01230 ± 0.0071

Table 3 k_{eff} of oxide core at the BOC and EOC

Library	k_{eff} at BOC	k_{eff} at EOC
ENDF/B-VIII.0	1.02362 ± 0.00006	1.00567 ± 0.00007
ENDF/B-VII.1	1.02610 ± 0.00006	1.00857 ± 0.00006
JENDL-4.0	1.02539 ± 0.00006	1.00876 ± 0.00007
Reported result (average) [3]	1.02860 ± 0.0062	1.01360 ± 0.0082

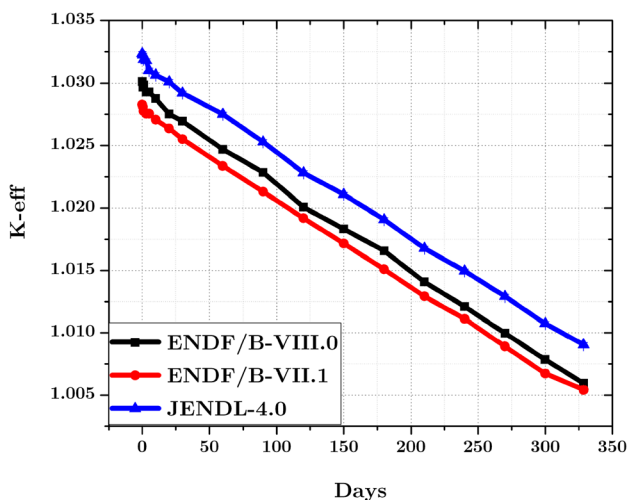


Fig. 3 (Color online) Effects of nuclear libraries on k_{eff} as a function of burnup for the SFR metallic core

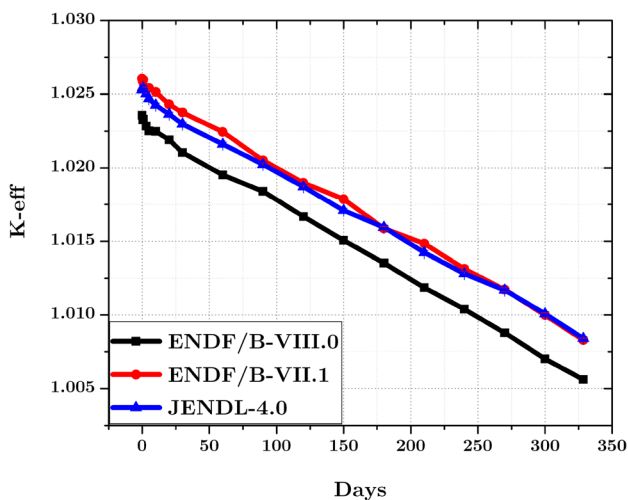


Fig. 4 (Color online) Effects of the nuclear libraries on k_{eff} as a function of burnup for the SFR oxide core

approximately 121 pcm (44-energy group) and 118 pcm (33-energy group) and is mostly contributed to by the fission reaction. However, the cross section of Fe-56 from ENDF/B-VIII.0 decreases the k_{eff} by approximately - 278 pcm (44-energy group) and - 276 pcm (33-energy group). It is also worth mentioning that both ENDF/B-VIII.0 and ENDF/B-VII.1 nuclear data have similar

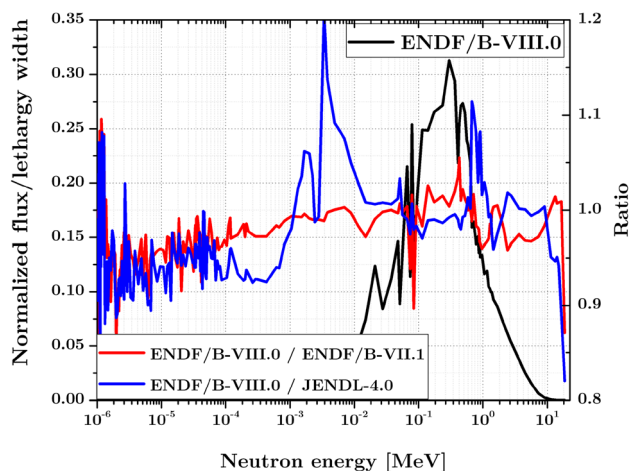


Fig. 5 (Color online) Effects of different nuclear libraries on the neutron spectra of SFR metallic core

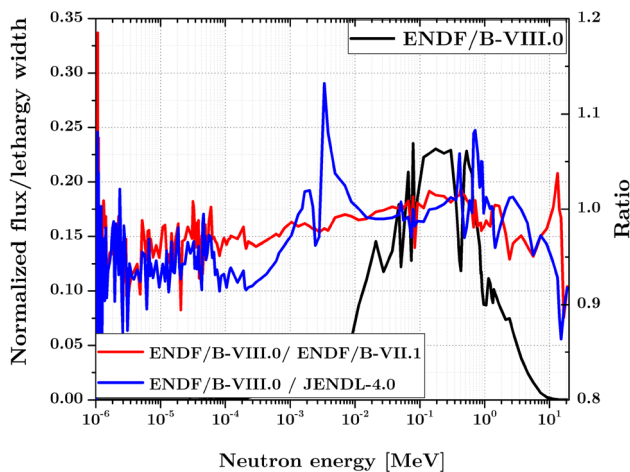


Fig. 6 (Color online) Effects of different nuclear libraries on the neutron spectra of the SFR oxide

inelastic scattering cross sections of Pu-239 in this core, which results in a zero discrepancy for the (n, inl) reaction.

Meanwhile, in the case of the JENDL-4.0 nuclear data library, it is shown that k_{eff} changes by approximately - 187 pcm (44-energy group) and - 180 pcm (33-energy group) when Fe-56 from ENDF/B-VIII.0 was used. A minor change of approximately - 1.2 pcm (44-energy group) and 7 pcm (33-energy group) was noted for U-238 from ENDF/B-VIII.0, which resulted from the balance between the positive contribution of (n, f) and (n, g) and the

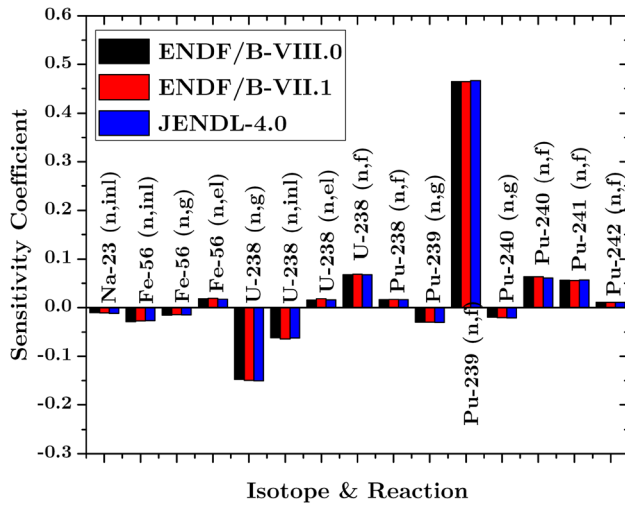


Fig. 7 (Color online) Sensitivity coefficient of metallic core for different nuclear data libraries

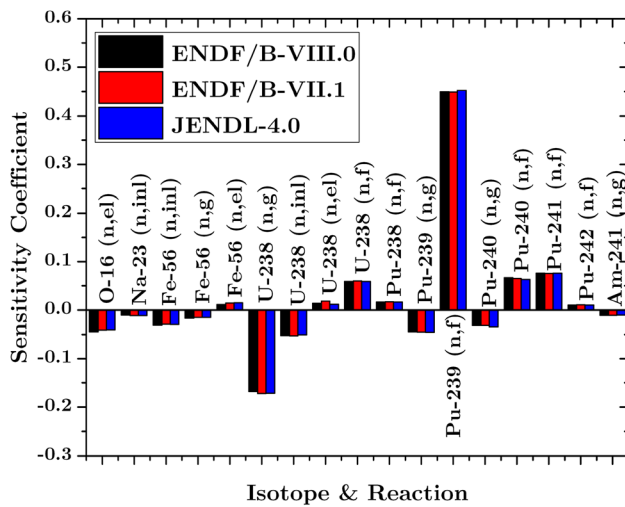


Fig. 8 (Color online) Sensitivity coefficient of oxide core for different nuclear data libraries

Table 4 Impact of the specific isotope library from ENDF/B-VIII.0 to k_{eff} of metallic core at BOC

Nuclear data	Isotope replaced by ENDF-B/VIII.0	Change (pcm)
ENDF/B-VII.1	Na-23	14 ± 7
	Fe-56	- 466 ± 7
	U-235	6 ± 7
	U-238	266 ± 7
	Pu-239	86 ± 7
	Am-241	8 ± 7
	JENDL-4.0	Na-23
	Fe-56	- 281 ± 7
	U-235	15 ± 7
	U-238	32 ± 7
	Pu-239	- 145 ± 7
	Am-241	- 94 ± 7

negative contribution of elastic and inelastic scattering reactions. Moreover, Pu-239 from ENDF/B-VIII.0 increased k_{eff} by approximately 22 pcm (44-energy group) and 18 pcm (33-energy group), which was mainly due to the enhancement in the fission reaction. These results for both ENDF/B-VII.1 and JENDL-4.0 are consistent with the trends in Tables 4, 5. A smaller discrepancy is noted owing to the use of a multi-energy group determine the contribution of each reaction to the k_{eff} .

Based on the results for the oxide core in Tables 8, 9, replacing the Fe-56 cross section from ENDF/B-VII.1 to the ENDF/B-VIII.0 library has a negative contribution to k_{eff} (- 350 pcm for the 44 energy group and - 353 pcm for the 33 energy group), whereas the contribution of U-238 was increased (170 pcm for the 44-energy group and 123 pcm for the 33-energy group). Moreover, the change in keff by Pu-239 was minor (9 pcm for the 44-energy group and - 9 pcm for the 33-energy group) owing to the balance between the increment in the fission reaction and the decrement in the (n,g) reaction. By contrast, replacing JENDL-4.0 with the new library (ENDF/B-VIII.0) revealed a smaller contribution for U-238 (41 pcm for the 44-energy group and 34 pcm for the 33-energy group). The contribution of Fe-56 from the new nuclear data decreases k_{eff} by approximately - 231.03 and - 238.61 pcm for the 44-energy group and 33-energy group, respectively. Meanwhile, Pu-239 from ENDF/B-VIII.0 showed a decrease in k_{eff} of approximately - 157 pcm for the 44-energy group and - 169 pcm for the 33-energy group.

Tables 10, 11 illustrate the differences between the 44-energy group and 33-energy-group structures. The highest contribution was recorded for U-238 using the ENDF/B-VII.1 library for both the metallic and the oxide cores, which was mainly caused by the inelastic neutron scattering reaction, which is dominant in the fast spectrum

Table 5 Impact of the specific isotope library from ENDF/B-VIII.0 to k_{eff} of oxide core at BOC

Nuclear data	Isotope replaced by ENDF-B/VIII.0	Change (pcm)
ENDF/B-VII.1	O-16	- 33 ± 9
	Na-23	- 8 ± 9
	Fe-56	- 569 ± 9
	U-235	- 14 ± 9
	U-238	205 ± 9
	Pu-239	- 42 ± 9
JENDL-4.0	Am-241	- 10 ± 9
	O-16	16 ± 9
	Na-23	96 ± 9
	Fe-56	- 348 ± 9
	U-235	13 ± 9
	U-238	78 ± 9

Table 6 Major contributors to change in k_{eff} of the metallic core using 33-energy group (unit in pcm)

Nuclear data	Isotope replaced by ENDF/B-VIII.0	Reaction				Resultant change
		(n,el)	(n,inl)	(n,f)	(n,g)	
ENDF/B-VII.1	Fe-56	- 7.30	- 151.06	-	- 118.29	- 276.65
	U-238	- 8.75	- 77.95	99.06	123.04	135.40
	Pu-239	0.14	0.03	154.15	- 36.08	118.25
JENDL-4.0	Fe-56	- 19.46	- 95.86	-	- 65.51	- 180.84
	U-238	- 11.38	- 284.92	118.37	185.15	7.22
	Pu-239	- 3.01	- 11.92	26.24	7.49	18.80

Table 7 Major contributors to change in k_{eff} of the metallic core using 44-energy group (unit in pcm)

Nuclear data	Isotope replaced by ENDF/B-VIII.0	Reaction				Resultant change
		(n,el)	(n,inl)	(n,f)	(n,g)	
ENDF/B-VII.1	Fe-56	- 7.32	- 153.89	-	- 117.25	- 278.47
	U-238	- 0.94	- 47.30	102.18	121.12	175.07
	Pu-239	- 0.23	0.00	163.34	- 42.05	121.05
JENDL-4.0	Fe-56	- 19.09	- 108.86	-	- 59.37	- 187.32
	U-238	- 7.17	- 277.79	111.89	171.87	- 1.21
	Pu-239	- 5.92	- 14.67	36.74	6.39	22.53

region, resulting in more energy groups (44 instead of 33), resulting in a significant difference in this case. However, the difference between using the 44-energy group and the 33-energy group is relatively small and slightly higher for the oxide core than that of the metallic core.

5.4 Kinetic parameters

The calculated kinetic parameters, i.e., a prompt neutron generation time Λ and the total effective delayed neutron

fraction β_{eff} at BOC and EOC, are shown in Figs. 9, 10 respectively. The parameters are adjoint-weighted values calculated using the iterated fission probability method implemented in SERPENT2. The prompt neutron generation time of the metallic core is shorter than that of the oxide core owing to the harder spectrum in the metallic core, whereas the total effective delayed neutron fraction of the metallic core is higher than that of the oxide core because of the lower amount of Pu and the minor actinide in the metallic core. It should be noted that the three

Table 8 Major contributors to the change in k_{eff} of the oxide core using 33-energy group (unit in pcm)

Nuclear data	Isotope by ENDF-B/VIII.0	Reaction				Resultant change
		(n,el)	(n,inl)	(n,f)	(n,g)	
ENDF/B-VII.1	Fe-56	- 8.35	- 160.86	-	- 183.80	- 353.01
	U-238	- 6.53	- 64.26	78.02	115.99	123.22
	Pu-239	- 0.29	0.06	35.35	- 44.39	- 9.27
JENDL-4.0	Fe-56	- 12.19	- 101.78	-	- 124.64	- 238.61
	U-238	- 4.37	- 215.75	100.91	154.00	34.80
	Pu-239	0.62	- 7.99	- 118.77	- 43.11	- 169.25

Table 9 Major contributors to change in k_{eff} of the oxide core using 44-energy group (unit in pcm)

Nuclear data	Isotope by ENDF-B/VIII.0	Reaction				Resultant change
		(n,el)	(n,inl)	(n,f)	(n,g)	
ENDF/B-VII.1	Fe-56	- 7.11	- 164.99	-	- 178.20	- 350.31
	U-238	6.64	- 41.05	82.19	123.02	170.81
	Pu-239	0.46	0.04	53.31	- 44.44	9.37
JENDL-4.0	Fe-56	- 9.95	- 106.99	-	- 114.10	- 231.03
	U-238	- 2.41	- 208.27	92.45	159.26	41.02
	Pu-239	2.35	-7.69	-107.69	-44.43	-157.46

Table 10 Difference in the major contributors to k_{eff} between 44-energy group and 33-energy group for metallic core (unit in pcm)

Nuclear data	Isotope by ENDF – B/VIII.0	Reaction				Resultant change
		(n,el)	(n,inl)	(n,f)	(n,g)	
ENDF/B-VII.1	Fe-56	- 0.02	- 2.83	-	1.04	- 1.82
	U-238	7.81	30.65	3.12	- 1.92	39.67
	Pu-239	- 0.37	- 0.03	9.19	- 5.97	2.8
JENDL-4.0	Fe-56	0.37	- 13	-	6.14	- 6.48
	U-238	4.21	7.13	- 6.48	- 13.28	- 8.43
	Pu-239	- 2.91	- 2.75	10.5	- 1.1	3.73

Table 11 Difference in the major contributors to k_{eff} between 44-energy group and 33-energy group for oxide core (unit in pcm)

Nuclear data	Isotope by ENDF-B/VIII.0	Reaction				Resultant change
		(n,el)	(n,inl)	(n,f)	(n,g)	
ENDF/B-VII.1	Fe-56	1.24	- 4.13	-	5.6	2.7
	U-238	13.17	23.21	4.17	7.03	47.59
	Pu-239	0.75	- 0.02	17.96	- 0.05	18.64
JENDL-4.0	Fe-56	2.24	- 5.21	-	10.54	7.58
	U-238	1.96	7.48	- 8.46	5.26	6.22
	Pu-239	1.73	0.3	11.08	- 1.32	11.79

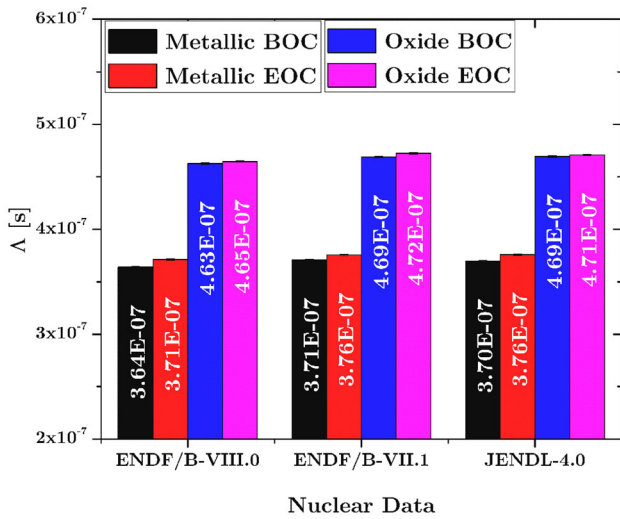


Fig. 9 (Color online) Λ of both cores for different nuclear data libraries

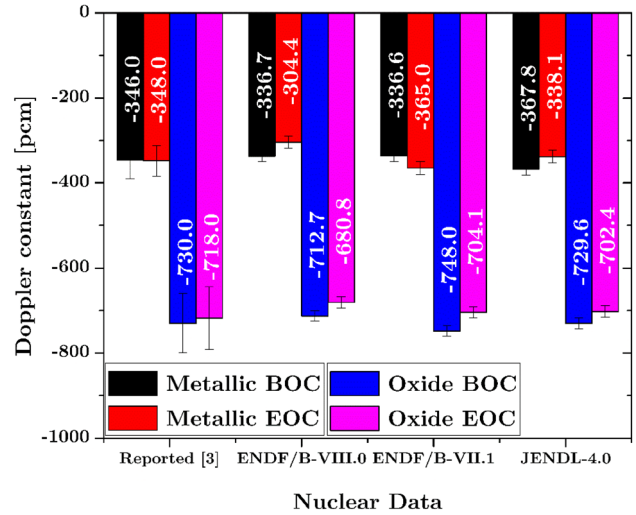


Fig. 11 (Color online) Doppler constant K_D for different libraries and both SFR cores

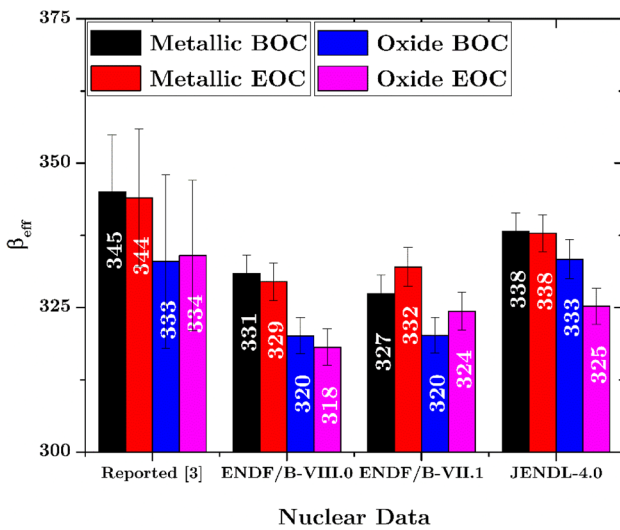


Fig. 10 (Color online) β_{eff} of both cores for different nuclear data libraries

different libraries produce similar and consistent kinetic parameters. Meanwhile, the β_{eff} reported [3] is slightly higher than the calculated values. The benchmark results are summarized in Table 12.

5.5 Doppler constant K_D

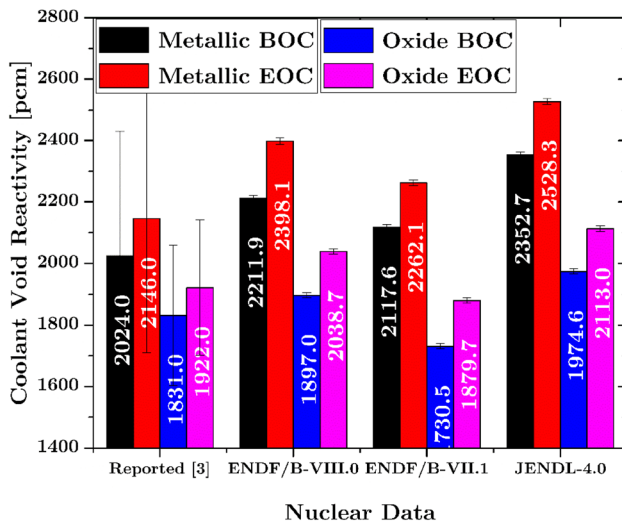
Figure 11 shows the Doppler constant K_D for both cores at the BOC and EOC. It is defined as the difference in reactivity when the fuel temperature is doubled and at a normal fuel operating temperature. It is clearly shown that the oxide core has a more negative K_D than the metallic core owing to the softer spectrum in the oxide core. Moreover, the oxide core contains more U-238 than the metallic core. It is also noted that the three different libraries have similar and consistent K_D values. Meanwhile, the reported K_D [3] is also slightly higher than the calculated value. Table 13 summarizes the benchmark results.

Table 12 β_{eff} of both cores for different nuclear data library benchmark results

Core	Condition	Reported result (average value) [3] (pcm)	ENDF/B-VIII.0 (pcm)
Metallic	BOC	345 ± 10	331 ± 3
	EOC	344 ± 12	329 ± 3
Oxide	BOC	333 ± 15	320 ± 3
	EOC	334 ± 13	318 ± 3

Table 13 Doppler constant K_D of both cores for different nuclear data library benchmark results

Core	Condition	Reported result (average value) [3] (pcm/K)	ENDF/B-VIII.0 (pcm/K)
Metallic	BOC	-346 ± 44	-337 ± 14
	EOC	-348 ± 36	-340 ± 15
Oxide	BOC	-730 ± 70	-713 ± 12
	EOC	-718 ± 74	-681 ± 13

**Fig. 12** (Color online) CVR for different libraries and both SFR cores**Table 14** CVR for different libraries and benchmark results of both SFR cores

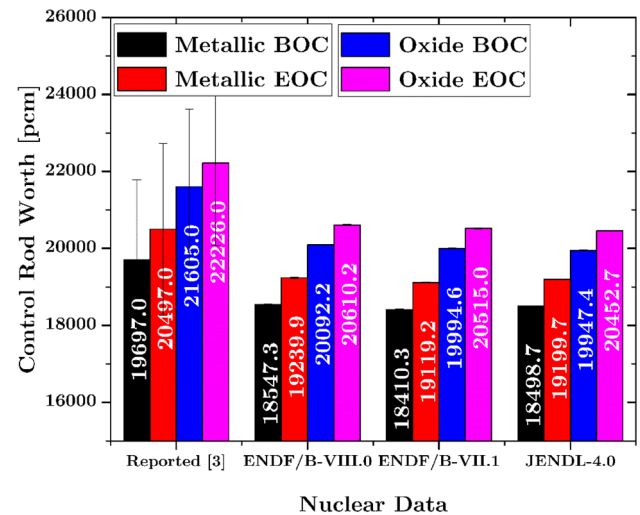
Core	Condition	Reported result (average value) [3] (pcm)	ENDF/B-VIII.0 (pcm)
Metallic	BOC	2024 ± 407	2212 ± 10
	EOC	2146 ± 435	2398 ± 10
Oxide	BOC	1831 ± 228	1897 ± 9
	EOC	1922 ± 220	2039 ± 9

5.6 CVR

The CVR is summarized in Fig. 12 for both cores at the BOC and EOC. It is defined as the difference in reactivity when the coolant is voided and under normal conditions. It is clearly shown that the metallic core is more positive (CVR) than the oxide core because of the harder spectrum shown in the metallic core. It should also be noted that the three different libraries have similar and consistent CVR values. Meanwhile, the reported CVR values [3] are lower than the calculated values except for the oxide core using ENDF/B-VII.1. Table 14 summarizes the benchmark results.

5.7 CR worth

The last result, which is the CR worth, is shown in Fig. 13, which is calculated as the reactivity difference

**Fig. 13** (Color online) CR worth of both cores for different nuclear data libraries

when all control subassemblies are withdrawn and inserted. It should also be noted that the three different libraries give similar and consistent CR values. Meanwhile, the reported CR value [3] is higher than the calculated values. Table 15 summarizes the benchmark results.

6 Summary and conclusions

In this study, the impact of the newly released ENDF/B-VIII.0 nuclear data library on the neutronics and kinetics parameters of two different spectra, namely metallic and oxide SFR cores, was studied. The newly released Fe-56 cross section, particularly its (n, inl) and (n, g) cross sections, shows a significant reduction in k_{eff} compared to those with ENDF/B-VII.1 and JENDL-4.0. In addition, a sensitivity analysis study revealed the major contributors to the resultant change in k_{eff} . Another significant impact

Table 15 CR worth for different libraries and benchmark results of both SFR cores

Core	Condition	Reported result (average value) [3] (pcm)	ENDF/B-VIII.0 (pcm)
Metallic	BOC	19,697 ± 2087	18,547 ± 12
	EOC	20,497 ± 2228	19,240 ± 14
Oxide	BOC	21,605 ± 2021	20,092 ± 12
	EOC	22,226 ± 2157	20,610 ± 13

includes the U-238 of ENDF/B-VII.1 and Pu-239 of JENDL-4.0. By contrast, the values of the kinetic parameters, Doppler constant, CVR, and CR worth between libraries were found to be consistent.

References

- N.E. Stauff, T.K. Kim, T.A. Taiwo et al., Benchmark for neutronic analysis of sodium-cooled fast reactor cores with various fuel types and core sizes. NEA-NSC-R-2015-9, Organization for economic co-operation and development (2016)
- L. Buiron, G. Rimpault, B. Fontaine et al., Evaluation of large 3600 MWth sodium-cooled fast reactor OECD neutronic benchmarks. In Proc. PHYSOR 2014 (2014)
- L. Buiron, L. G. Rimpault, B. Fontaine et al., Evaluation of large 1000 MWth sodium-cooled fast reactor OECD neutronic benchmarks. In Proc. PHYSOR 2014 (2014)
- M.B. Chadwick, P. Obložinský, M. Herman et al., ENDF/B-VII. 0: next generation evaluated nuclear data library for nuclear science and technology. Nucl. Data Sheets **107**(12), 2931–3060 (2014). <https://doi.org/10.1016/j.nds.2006.11.001>
- M.B. Chadwick, M. Herman, M.P. Obložinský et al., ENDF/B-VII. 1 nuclear data for science and technology: cross sections, covariances, fission product yields and decay data. Nucl. Data Sheets **112**(12), 2887–2996 (2011). <https://doi.org/10.1016/j.nds.2011.11.002>
- A. Koning, R. Forrest, M. Kellett et al., The JEFF-3.1 nuclear data library-JEFF report 21. NEA-6190, Organisation for economic co-operation and development (2006)
- K. Shibata, O. Iwamoto, T. Nakagawa et al., JENDL-4.0: a new library for nuclear science and engineering. J. Nucl. Sci. Technol. **48**(1), 1–30 (2011). <https://doi.org/10.1080/18811248.2011.9711675>
- D.A. Brown, M.B. Chadwick, R. Capote et al., ENDF/B-VIII. 0: the 8th major release of the nuclear reaction data library with CIELO-project cross sections, new standards and thermal scattering data. Nucl. Data Sheets **148**, 1–142 (2018). <https://doi.org/10.1016/j.nds.2018.02.001>
- J. Leppänen, M. Pusa, T. Viitanen et al., The Serpent Monte Carlo code: Status, development and applications in 2013. Ann. Nucl. Energy **82**, 142–150 (2014). <https://doi.org/10.1016/j.anucene.2014.08.024>
- E. Woodcock, T. Murphy, P. Hemmings, et al., Techniques used in the GEM code for Monte Carlo neutronics calculations in reactors and other systems of complex geometry. In Proc. Conf. applications of computing methods to reactor problems, ANL-7050, page 557, Argonne National Laboratory (1965)
- J. Leppänen, Performance of Woodcock delta-tracking in lattice physics applications using the serpent Monte Carlo reactor physics burnup calculation code. Ann. Nucl. Energy **37**(5), 715–722 (2010). <https://doi.org/10.1016/j.anucene.2010.01.011>
- B. Becker, R. Dagan, G. Lohnert, Proof and implementation of the stochastic formula for ideal gas, energy dependent scattering kernel. Ann. Nucl. Energy **36**(4), 470–474 (2009). <https://doi.org/10.1016/j.anucene.2008.12.001>
- C.H. Lee, W.S. Yang. MC²-3: multigroup cross section generation code for fast reactor analysis, ANL/NE-11-41 Rev.2, Argonne National Laboratory (2013)
- M. Aufiero, A. Bidaud, M. Hursin et al., A collision history-based approach to sensitivity/perturbation calculations in the continuous energy Monte Carlo code serpent. Ann. Nucl. Energy **85**, 245–258 (2015). <https://doi.org/10.1016/j.anucene.2015.05.008>